Characterization of Helical Propulsion Inside *In Vitro* and *Ex Vivo* Models of a Rabbit Aorta

Dalia Mahdy*, Sarah Hesham†, Mohannad Mansour*
Abdallah Mohamed*, Ibrahim Basla†, Nabila Hamdi†, Islam S. M. Khalil‡, and Sarthak Misra‡§

***Abstract*— In this work, the propulsion of a helical robot is experimentally characterized inside whole blood (*in vitro* model) and against the flowing streams of phosphate buffered saline (PBS) inside rabbit aorta (*ex vivo* model). The helical robot is magnetically actuated inside these models under the influence of rotating magnetic fields. The frequency response of the helical robot is characterized. Averaged speed is measured at actuation frequency of 8 Hz as 11.3 ± 0.52 (*n* = 5) and 7.45 ± 1.2 mm/s (*n* = 3) inside rabbit aorta and whole blood, respectively. The Speed of the robot inside rabbit aorta is characterized against flowing streams of PBS at flow rate of 90 ml/hr.**

I. Introduction

Characterization of micro and nanorobots inside *in vitro* and *ex vivo* models is essential for their translation into biomedical applications. These devices are powered and controlled remotely using externally-applied magnetic fields for motion control in two- and three-dimensional space. Drug delivery [1], micro-assembly [2], transportation and manipulation of biological cells [3], and diagnostics and bio-detection [4] have been demonstrated using microrobots. Felfoul *et al.* have utilized magnetotactic bacteria to enhance the therapeutic index during targeted therapy *in vivo*. They have employed the migration behaviour of *Magnetococcus marinus* strain MC-1 for their control towards a desired location [5]. Vonthron et al. have also demonstrated motion control of microrobots using a clinical magnetic resonance imaging system. They have implemented steering and localization of microrobots to achieve controlled navigation inside narrow blood vessels [6]. Also, A swarm of functionalized artificial bacterial flagella has been controlled *in vivo* using rotating magnetic fields based on the feedback of an optical fluorescence imaging system by Servant *et al.* [7]. Propulsion of drug-loaded magnesium microrobots have been demonstrated inside the gastric media of a mouse model by Fernndez de vila *et al.* [8]. Although the mentioned results are promising, the conditions that will be encountered inside the human body are more challenging. For instance, the average blood flow rate in adults through the carotid artery is approximately 350 ml/min and 750 ml/min through the whole brain [9]. Motion control of microrobots against such flow rates has not been achieved yet. In addition, the thrombogenic response of the material of the microrobot will likely influence its locomotion in blood vessels. For instance, a microrobot with relatively high thrombogenic (such as titanium and tantalum) is expected to be surrounded with platelets while swimming in blood, and hence the swimming speed is expected to decrease as the drag force will increase for the same propulsive force.

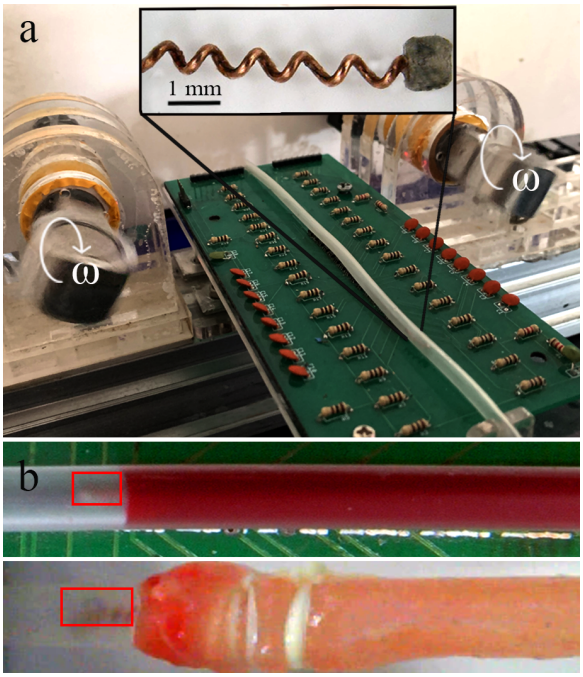

Fig. 1. Helical propulsion is characterized inside *in vitro* and *ex vivo* models. (a) The actuation of a helical robot (inset) is achieved using two synchronized rotating dipole fields. (b) The robot swims in whole blood inside a catheter segment with averaged speed of 7.45 ± 1.2 mm/s (*n* = 3) at actuation frequency of 8 Hz. (c) An aorta is dissected from a rabbit and the averaged speed of the helical robot is measured as 11.3 ± 0.52 mm/s (*n* = 5) against flowing streams of phosphate buffered saline at actuation frequency of 8 Hz.

In this work, the propulsion of a helical robot is experimentally characterized inside *in vitro* and *ex vivo* models. The helical robot is actuated by a permanent magnet-based robotic system using two synchronized rotating dipole fields [10], and we achieve the following:

- *in vitro* characterization of the frequency response of a helical robot inside a blood-filled catheter segment, using an array of Hall-effect sensors for localization.
- *ex vivo* characterization of the frequency response of a helical robot inside an isolated rabbit aorta, against the

The authors are affiliated with the *Department of Mechatronics Engineering, †Faculty of Pharmacy and Biotechnology, the German University in Cairo, New Cairo 11835, Egypt.

‡The authors are affiliated with the Department of Biomechanical Engineering, University of Twente, Enschede 7500 AE, The Netherlands.

§Department of Biomedical Engineering, University of Groningen and University Medical Centre Groningen, Groningen 9713 AV, The Netherlands.

978-1-5386-1311-5/19/$31.00 ©2019 IEEE

flowing streams of phosphate buffered saline (PBS) at flow rate of 90 ml/hr.

The remainder of this paper is organized as follows: Section II provides descriptions pertaining to the magnetic-based robotic system, the *in vitro*, and *ex vivo* models implemented for experimental characterization. In addition, the influence of these models on the helical propulsion are discussed in the same Section. The experimental results are provided in Section III. Finally, Section V concludes and provides directions for future work.

II. Helical Propulsion and System Description

The helical robot is allowed to swim under the influence of two synchronized rotating dipole fields inside a blood-filled catheter segment and a segment of a dissected rabbit aorta. These fields are generated using a permanent magnet-based robotic system.

A. System Description

The helical robot is characterized using a permanent magnet-based robotic system. This system comprises two rotating permanent magnets (R750F, Amazing Magnets LLC, California, USA) to generate rotating magnetic fields. Each permanent magnet generates magnetic field of 0.552 T on its surface. These fields exert a magnetic torque on the dipole moment of the helical robot that is allowed to swim between the permanent magnets, and contained inside a catheter segment or a rabbit aorta. The robot consists of a magnetic head and a tail. The head is a cylindrical permanent magnet (S-01-01-N, Supermagnete, Gottmadingen, Germany) and the tail is a helix-shaped copper wire (length, diameter, and pitch of 4 mm, 0.2 mm, and 0.85 mm, respectively). The head is attached rigidly to the tail such that its magnetization axis is orthogonal to the helix axis. Rotation of the permanent magnets enables helical propulsion of the robot against the mentioned mediums. In the case of *in vitro* model, a polyvinyl chloride catheter segment is filled with the mediums, whereas in the *ex vivo* model a segment from the aorta is isolated from a rabbit and connected to catheters to provide flow.

B. Helical propulsion

The helical robot is propelled inside the catheter segment or the aorta using two rotating permanent magnets. The axes of rotation of the permanent magnets are parallel to the helical robot to achieve one-dimensional locomotion inside the segment. We calculate the Reynolds number as $Re = \frac{\rho_\mathrm{f}|\mathbf{U}|L}{\mu} \simeq 0.004$, where ρ_f is the density of the medium, $\mathbf{U}$ is the speed of the helical robot, L is its length, and μ is the dynamic viscosity of the medium. The calculated Reynolds number is in the order of $\mathcal{O}(10^{-3})$. In such low Reynolds numbers viscous forces are dominant. Based on the hydrodynamic model presented in [11], the governing equations are given by

$$\begin{pmatrix} \mathbf{F}_\mathrm{m} + \mathbf{F}_\mathrm{g} + \mathbf{F}_\mathrm{d} + \mathbf{F}_\mathrm{c} \\ \mathbf{T}_\mathrm{m} + \mathbf{T}_\mathrm{g} + \mathbf{T}_\mathrm{d} + \mathbf{T}_\mathrm{c} \end{pmatrix} = 0, \tag{1}$$

where $\mathbf{F}_\mathrm{m}$ and $\mathbf{T}_\mathrm{m}$ are the magnetic force and torque exerted on the dipole moment of the helical robot, respectively. Further, $\mathbf{F}_\mathrm{g}$ and $\mathbf{T}_\mathrm{g}$ are the force and torque exerted on the robot due to gravity, respectively. Furthermore, $\mathbf{F}_\mathrm{d}$ and $\mathbf{T}_\mathrm{d}$ are the drag force and torque, respectively, and $\mathbf{F}_\mathrm{c}$ and $\mathbf{T}_\mathrm{c}$ are the force and torque due to the contact of the robot with the channel wall, respectively. The influence of the contact forces on the helical propulsion can be neglected in the absence of contact with the channel walls or when the gravity is compensated using a vertical propulsive force component. This compensation is not possible in narrow channels as the robot becomes in continuous contact with the inner surface of the channel and constrained. In (1), the magnetic and gravitational forces and torques are given by

$$\begin{pmatrix} \mathbf{F}_\mathrm{m} \\ \mathbf{T}_\mathrm{m} \end{pmatrix} = \begin{pmatrix} (\mathbf{m}\cdot\nabla)\mathbf{B} \\ \mathbf{m}\times\mathbf{B} \end{pmatrix} \text{ and } \begin{pmatrix} \mathbf{F}_\mathrm{g} \\ \mathbf{T}_\mathrm{g} \end{pmatrix} = \begin{pmatrix} \rho\mathbf{R}^\mathrm{T}\mathbf{g} \\ \mathbf{r}\times\mathbf{F}_\mathrm{g} \end{pmatrix}, \tag{2}$$

where $\mathbf{B}$ and $\mathbf{m}$ are the magnetic field of the rotating dipole fields and the magnetic dipole moment of the helical robot, respectively. Further, $\rho = \rho_\mathrm{r} - \rho_\mathrm{f}$, where ρ_r is the density of the helical robot. Furthermore, $\mathbf{r} = \mathbf{r}_\mathrm{cov} - \mathbf{r}_\mathrm{com}$, where $\mathbf{r}_\mathrm{cov}$ and $\mathbf{r}_\mathrm{com}$ are the center of volume and center of mass of the robot, respectively. In (2), $\mathbf{R}$ and $\mathbf{g}$ are the rotation matrix between the robot and a frame of reference, and a vector of gravitational attraction, respectively. The drag and contact forces and torques are given by

$$\begin{pmatrix} \mathbf{F}_\mathrm{d} \\ \mathbf{T}_\mathrm{d} \end{pmatrix} = \mathbf{Z}\begin{pmatrix} \mathbf{U}+\mathbf{U}_\mathrm{ch} \\ \boldsymbol{\Omega} \end{pmatrix} \text{ and } \begin{pmatrix} \mathbf{F}_\mathrm{c} \\ \mathbf{T}_\mathrm{c} \end{pmatrix} = \begin{pmatrix} (k\beta + c\gamma)\,\mathbf{n}_\mathrm{c} \\ \mathbf{r}_\mathrm{c}\times\mathbf{F}_\mathrm{c} \end{pmatrix}, \tag{3}$$

where $\mathbf{Z}$ is a matrix that depends on the geometry of the helical robot and the properties of the fluid, U_ch and $\boldsymbol{\Omega}$ are the velocity field of the flow inside the channel and the angular velocity of the helical robot, respectively. Further, k and c are the stiffness and damping of the channel wall, respectively, and the coefficients β and γ are given by

$$\beta = \begin{cases} \delta, & \text{if } \delta \le 0 \\ 0, & \delta > 0 \end{cases} \text{ and } \gamma = \begin{cases} \frac{\mathrm{d}\delta}{\mathrm{d}t}, & \text{if } \frac{\mathrm{d}\delta}{\mathrm{d}t} > 0 \\ 0, & \frac{\mathrm{d}\delta}{\mathrm{d}t} \le 0 \end{cases}, \tag{4}$$

where δ is the penetration depth along the lateral direction. Further, $\mathbf{n}_\mathrm{c}$ and $\mathbf{r}_\mathrm{c}$ is the surface normal of the channel wall at the point of contact and the position vector of the contact point, respectively.

III. *In Vitro* and *Ex-Vivo* Characterization

The speed of a helical robot is characterized inside whole blood and a segment of a dissected rabbit aorta, under the influence of rotating magnetic fields with frequency range of 3 Hz to 8 Hz . All experiments are conducted at room temperature (25°C).

A. Characterization inside whole blood

Venous blood is drawn from a healthy donor (male 22 years old) into a vacutainer containing an anticoagulant (lithium heparin) to prevent blood clotting and keep the blood in its fluid form, and Local Institutional Ethical Board

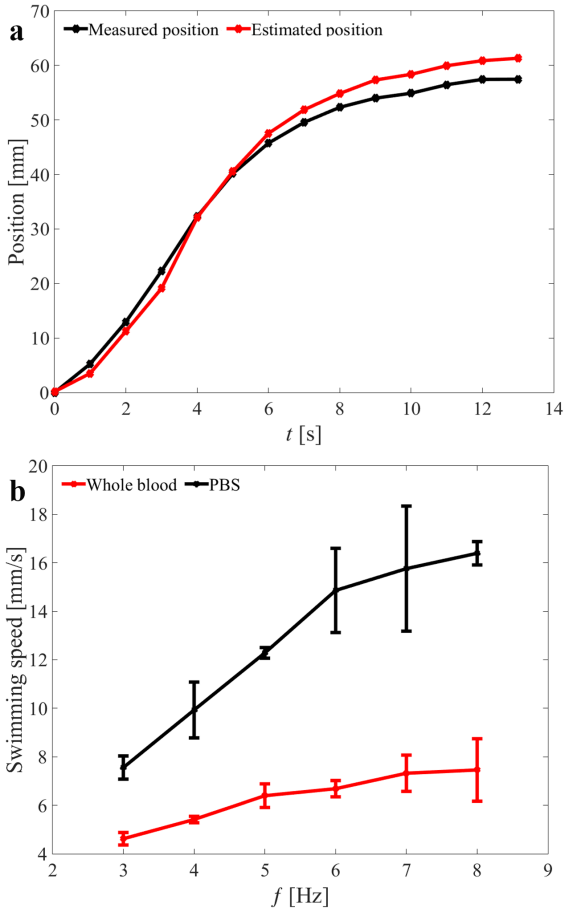

Fig. 2. Position of helical robot is localized during its propulsion inside a catheter segment under the influence of rotating magnetic fields [13]. (a) Position is measured and estimated using camera feedback and a magnetic localization system, respectively. The mean absolute error between the two methods is 2.2 ± 1 mm.(b) Speed of helical robot in whole blood is characterized under the influence of rotating magnetic fields with varying frequency in the range of 3 Hz to 8 Hz.

approval(2018-06-PBT-NH) is obtained for the collection and handling of the sample, and the donor has given written informed consent. An array of Hall-effect sensors is used to localize the helical robot and measure its speed as the robot is not visible in blood [13]. A representative trial for the localization of the helical robot in PBS is shown in Fig. 2(a). The mean absolute error between the measured position from camera feedback and the estimated position with the magnetic localization array, is calculated as 2.2 ± 1 mm from 3 trials of each method. Speed of the helical robot is characterized in whole blood and PBS without flow (Fig. 2(b)). The maximum speed is measured at frequency of 8 Hz as 16.3 ± 0.48 mm/s (n = 3) and 7.45 ± 1.2 mm/s (n = 3) in PBS and whole blood, respectively. The speed of helical robot is affected differently by the actuation frequency in whole blood than PBS, since PBS is devoid of blood components such as; blood cells, plasma, and proteins, which could increase the flow resistance inside the channel.

B. Characterization inside rabbit aorta

Aorta is an elastic artery with an expandable media for circulating blood. It consists of three main layers from inside to outside, i.e., *tunica intima*, *tunica media*, and *tunica adventitia* [14]. The inner layer *Tunica media* is the muscular layer of arteries and veins, it provides elasticity and controls the diameter of a blood vessel. In arteries, the *tunica adventitia* is supported by an external lamina that increases the elasticity needed for greater expansion in case of relatively higher flow rate. Such elastic properties affect the propulsion of the robot and its swimming speed inside the aorta. We characterize the speed of the helical robot in a segment of a rabbit aorta (Fig. 3(a)). A rabbit weighting 1.5 kg is dissected and its aorta is isolated. The ends of the aorta segment are connected to a catheter segment of 3 mm inner-diameter for PBS circulation. The aorta is connected to a syringe pump (Genie Plus, GT-4201D-12, Kent Scientific, Connecticut, USA) and a flow of 90 ml/hr is induced against the direction of propulsion, which maintains the viability of the aorta during the experiments. The diameter of the aorta is measured as 4 ± 0.3 mm, this variation in the diameter could be attributed to the elasticity of the aorta. Maximum speed of the robot in the aorta segment is achieved at actuation frequency of 8 Hz, and measured as 11.3 ± 0.52 mm/s versus 14.8 ± 0.37 mm/s in the catheter segment. Averaged speed and standard deviations are calculated from 5 trials (n = 5). A representative trial at actuation frequency of 7 Hz is shown in Fig. 3(b). The speed reduction inside the aorta segment in comparison to PBS could be attributed to the elastic properties of the aorta, and the interaction between the robot and the inner layer of the aorta compared to the interaction with the rigid channel wall of the catheter segment. In addition, the reduction in the swimming speed of the helical robot inside the catheter segment in Fig. 3(a) in comparison to Fig. 2(b), is attributed to the presence of a flow rate of 90 ml/hr against the direction of propulsion for comparison with swimming speed inside rabbit under the same settings.

A statistical test is conducted using analysis of variance (ANOVA) to investigate the influence of the actuation frequency, the host model (rabbit aorta and catheter segment), and the swimming medium (whole blood and PBS) on the swimming speed of helical robot. Results show statistical significance ($F_0 > F_\alpha$), where F_0 is calculated as 3.25 and 14.94 and F_α is calculated as 2.48 and 4.12 for the actuation frequency and the host model, respectively. In addition, the influence of the medium on swimming speed is statistically significant ($F_0 > F_\alpha$), where $F_0 = 8.42$ and $F_\alpha = 4.25$.

IV. CONCLUSIONS AND FUTURE WORK

The speed of a helical robot is experimentally characterized inside blood-filled catheter segment and a segment of an isolated rabbit aorta , under the influence of rotating magnetic fields with varying frequency in the range of 3 Hz to 8 Hz. The robot swims against a flow of PBS at 90 ml/hr with a maximum speed of 11.3 ± 0.52 mm/s inside the aorta compared to 14.8 ± 0.37 mm/s in catheter

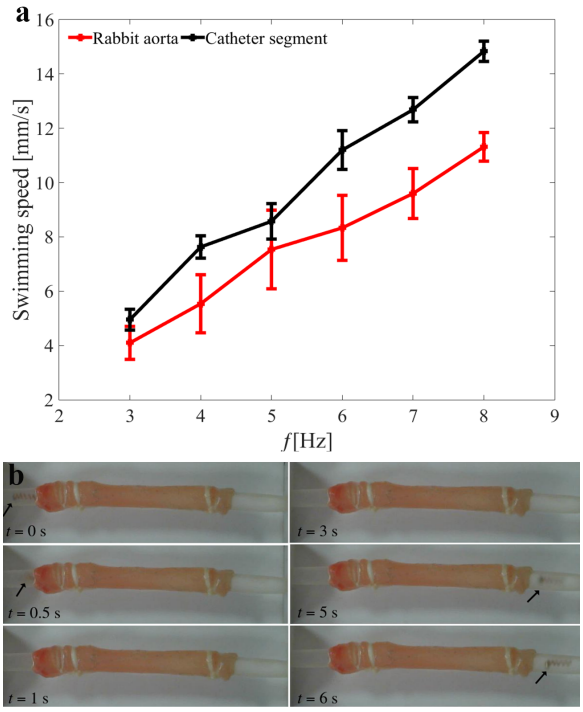

Fig. 3. The helical robot swims inside a dissected segment of a rabbit aorta with a diameter of 4 ± 0.3 mm. (a) The speed of the robot is characterized under the influence of rotating magnetic fields with frequency range of 3 Hz to 8 Hz. (b) A representative trial shows the actuation of the helical robot inside the aorta. The averaged speed of helical robot at actuation frequency of 7 Hz is measured as 9.59 ± 0.91 mm/s.

segment at frequency of 8 Hz. The outer-diameter of the aorta is measured as 4 ± 0.3 mm varying according to the expansion by the applied flow rate. We attribute the reduction of swimming speed to the elastic properties of the aorta in comparison to a rigid catheter segment. In addition, maximum speed of the robot in whole blood is calculated as 7.45 ± 1.2 mm/s compared to 16.3 ± 0.48 mm/s in PBS. Experimental results show that the propulsion of the robot is influenced by the properties of the surrounding channels. The swimming speed of the helical robot inside the catheter segment is relatively higher than the speed in the rabbit aorta segment. The robot is in continuous contact with the surface of the aorta. Therefore, it is subject to higher contact forces for the same propulsive force. This speed reduction can be mitigated by decreasing the contact between the robot and the channel wall. In our experiments, the force due to gravity is not compensated. Gravity compensation using a vertical propulsive force component can decrease the contact with the channel wall during helical propulsion. In addition, the composition of *in vivo* swimming mediums such as whole blood affects the speed of the robot in comparison to swimming fluids used in *in vitro* experiments such as PBS.

As part of future studies, we will characterize the mechanical properties of the blood vessels and develop a model to simulate the behaviour of the helical robot and understand its response to conditions encountered *in vivo*. In addition, propulsion of the helical robot will be tested against higher flow rates than 90 ml/hr and we will investigate methods to enhance the propulsive force of the robot. It is also essential to fabricate the robot from a biodegradable material and use a coating with relatively low thrombogenic response to decrease the formation of platlets on the surface of the robot to be suitable for *in vivo* applications.

V. Acknowledgment

This work was supported by the European Research Council under the European 241 Unions Horizon 2020 Research and Innovation program under Grant 638428 - project 242 ROBOTAR: Robot-Assisted Flexible Needle Steering for Targeted Delivery of Magnetic 243 Agents.

References

[1] S. K. Srivastava, M. Medina-Sànchez, B. Koch, and O. G. Schmidt, "Medibots: Dual-action biogenic microdaggers for single-cell surgery and drug release," *Advacned Materials*, vol. 28, no. 5, pp. 832-837, November 2015.

[2] S. Martel and M. Mohammadi, "Using a swarm of self-propelled natural microrobots in the form of flagellated bacteria to perform complex microassembly tasks," in *Proceedings of the IEEE International Conference on Robotics and Automation (ICRA)*, pp. 500–505, March 2010.

[3] S. Sanchez, A. A. Solovev, S. Schulze, and O. G. Schmidt, "Controlled manipulation of multiple cells using catalytic microbots," *Chemical Communications*, vol. 47, no. 2, pp. 698–700, January 2011.

[4] S. Campuzano, D. Kagan, J. Orozco, and J.Wang, "Motion-Driven sensing and biosensing using electrochemically propelled nanomotors," *Analyst*, vol. 136, pp. 4621–4630, September 2011.

[5] O. Felfoul, M. Mohammadi, S. Taherkhani, D. D. Lanauze, Y. Z. Xu, D. Loghin, S. Essa, S. Jancik, D. Houle, M. Lafleur, L. Gaboury, M. Tabrizian, N. Kaou, M. Atkin, T. Vuong, G. Batist, N. Beauchemin, D. Radzioch, and S. Martel, "Magneto-aerotactic bacteria deliver drugcontaining nanoliposomes to tumour hypoxic regions," *Nature Nanotechnology*, vol. 11, pp. 941–947, August 2016.

[6] M. Vonthron, V. Lalande, G. Bringout, C. Tremblay, and S. Martel, "A MRI-based integrated platform for the navigation of microdevices and microrobots," in *Proceedings of the IEEE International Conference on Intelligent Robots and Systems (IROS)*, pp. 1285–1290 San Francisco, CA, USA, September 2011.

[7] A. Servant, F. Qiu, M. Mazza, K. Kostarelos, and B. J.Nelson, "Controlled in vivo swimming of a swarm of bacteria-like microrobotic flagella," *Advanced Materials*, vol. 27, no. 19, pp. 2981–2988, April 2015.

[8] B. Esteban-Fernndez de vila, P. Angsantikul, J. Li, M. A. Lopez-Ramirez, D. E. Ramrez-Herrera, S. Thamphiwatana, C. Chen, J. Delezuk, R. Samakapiruk, V. Ramez, M. Obonyo, L. Zhang, and J. Wang, "Micromotor-enabled active drug delivery for in vivo treatment of stomach infection," *Nature Communications*, vol. 8, no. 1, August 2017.

[9] E. R. Kandel, J, H. Schwartz, and T. M. Jessell, Principles of Neural Science (4th ed.), McGraw-Hill Medical, New York, 2000.

[10] A. Hosney, A. Klingner, S. Misra, and I. S. M. Khalil, "Propulsion and steering of helical magnetic microrobots using two synchronized rotating magentic field in three-dimensional space," in *Proceedings of the IEEE International Conference on Intelligent Robots and Systems (IROS)*, pp. 1988–1993, Hamburg, Germany, November 2015.

[11] I. S. M. Khalil, A. F. Tabak, K. Sadek, D. Mahdy, N. Hamdi, and M. Sitti, "Rubbing against blood clots using helical robots: Modeling and in vitro experimental validation," *IEEE Robotics and Automation Letters*, vol. 2, no. 2, pp. 927–934, April 2017.

[12] D. S. M. Guzman, M. A. Mitchell, S. D. Gaunt, D. Stephen, H. Beaufrère and T. N. Tully Jr, "Comparison of Hematologic Values in Blood Samples with lithium Heparin or Dipotassium Ethylenediaminetetraacetic Acid Anticoagulants in Hispaniolan Amazon Parrots (Amazona ventralis)," *Journal of Avian Medicine and Surgery,* vol. 22, no. 2, pp. 108–113, June 2008.

[13] A. Adel, M. Mansour, M. M. Micheal, A. Hassan, I. S. M. Khalil, and S. Misra, "Magnetic Localization for an Electromagnetic-Based Haptic Interface," *IEEE Magnetics Letters,* vol. 22, March 2019.

[14] P. A. Iaizzo, Handbook of Cardiac Anatomy, Physiology, and Devices, Springer, New York, 2009.